Amplification of a Surface-Intensified Eddy Drift along a Steep Shelf in the Eastern Mediterranean Sea

GEORGI SUTYRIN

Graduate School of Oceanography, University of Rhode Island, Narragansett, Rhode Island

ALEXANDER STEGNER

Laboratoire de Météorologie Dynamique, Centre National de la Recherche Scientifique, Ecole Normale Supérieure, Paris, France

ISABELLE TAUPIER-LETAGE

Université de la Méditerranée, Centre National de la Recherche Scientifique, Centre d'Océanologie de Marseille, La Seyne, France

SAMUEL TEINTURIER

Laboratoire de Météorologie Dynamique, Centre National de la Recherche Scientifique, Ecole Normale Supérieure, Paris, and Unité de Mecaniqué, Ecole National Supérieure des Techniques Avancées, Palaiseau, France

(Manuscript received 29 July 2008, in final form 3 February 2009)

ABSTRACT

The datasets of the Eddies and Gyre Path Tracking (EGYPT)/EGITTO program in the eastern Mediterranean Sea reveal a large mesoscale anticyclone traveling along the Libyan shelf. Surface drifter trajectories combined with a CTD transect accurately quantify the horizontal velocity and the vertical structure of this surface-intensified anticyclone. The observed westward drift speed is significantly higher than expected from the beta effect alone. To study the impact of a steep shelf topography on the propagation of compact surface-intensified vortices, the authors used a two-layer beta-plane model with steep continental slope and nearly zonal boundary. A perturbation theory derived by G. Sutyrin for a circular vortex in the upper layer with the lower layer at rest as a basic state is generalized for nonuniform slope in the presence of the image effect. An integral momentum balance is used to derive the drifting velocity of an upper-layer vortex with the main assumption that a stable and steady drifting solution of the two-layer system exists. The interface is described by a steady drifting circular dome at the leading order. This approach allows the problem to be reduced to the calculation of the deep-flow pattern, depending on the interface shape and topography. When the topographic slope beneath the eddy changes rapidly from a steep continental slope to a gentle continental rise, most of the deep-flow pattern is shifted offshore. The corresponding anticyclonic deep-flow feedback provides an additional along-slope propagation, which is proportional to the basic drift speed and the steepness parameter.

1. Introduction

Surface-intensified baroclinic eddies are often affected by continental slopes. Recent observations of the Eddies and Gyre Path Tracking (EGYPT)/EGITTO program quantify the horizontal and the vertical structure of a surface anticyclonic eddy drifting along the Libyan shelf. However, there is limited understanding of the leading dynamical processes interacting in large-scale eddies with steep topography. The aim of this paper is to clarify dominant physical mechanisms that are crucial for modeling eddy evolution in the presence of steep bathymetry and horizontal boundaries. We focus this study on surface-intensified eddies interacting with topography of limited lateral extent (e.g., continental slopes with steep gradients), as opposed to slowly varying topography, which has been the subject of some recent developments.

a. Background

Eddies or rings of the western boundary currents are among the most intense oceanic localized structures,

Corresponding author address: Georgi Sutyrin, Graduate School of Oceanography, University of Rhode Island, 215 South Ferry Road, Narragansett, RI 02882.
E-mail: gsutyrin@gso.uri.edu

DOI: 10.1175/2009JPO4106.1

© 2009 American Meteorological Society

and there is a large amount of observational evidence that they are typically transformed when they encounter continental slopes and shelves. Examples were described for Gulf Stream rings (Evans et al. 1985; Brown et al. 1986), Loop Current rings in the Gulf of Mexico (Kirwan et al. 1988; Vukovich and Waddell 1991), North Brazil Current rings (Fratantoni et al. 1995), North Pacific eddies (Umatani and Yamagata 1987), East Australian Current rings (Hamon 1965; Freeland et al. 1986), etc. These observations do not easily lend themselves to a canonical description of either the interaction processes or its results. These rings or eddies may remain near the shelf break or move offshore (Puillat et al. 2002), and there may be significant modification of the shelf water mass. In particular, our observations of eddy evolution in the vicinity of nearly zonal boundaries indicate along-slope drift essentially faster than expected from the beta effect alone (Fig. 1).

This variability of eddy interactions with continental slope and shelves indicates that there should be a number of variables that govern these interactions, and a number of authors have contributed theoretical insight likely to be relevant in explaining the behaviors observed. Some of the earliest studies of vortex–topography interactions have used a depth-averaged barotropic model [e.g., Firing and Beardsley (1976), Louis and Smith (1982), and Grimshaw et al. (1994) demonstrated the rapid dispersion of eddies into topographic Rossby waves over a steep continental slope]. Reorganization of the barotropic vortex structure resulting from various topographic effects was considered in a number of laboratory, numerical, and theoretical studies (e.g., Carnevale et al. 1991; Wang 1992; van Heijst 1994; McDonald 1998; van Geffen and Davies 1999; Richardson 2000).

The real ocean is stratified and baroclinic rings are typically surface intensified, so that their main core is not in direct contact with the topography. The deep-flow feedbacks on their evolution were often modeled using two-layer models with topographic slopes represented by a variable depth in the lower layer (e.g., Smith and O'Brien 1983; Smith 1986; Kamenkovich et al. 1996; Thierry and Morel 1999; Reznik and Sutyrin 2001; Sutyrin 2001; Jacob et al. 2002; Kizner et al. 2003; Sutyrin et al. 2003; Sutyrin and Grimshaw 2005).

In contrast with the studies focused on the deep-flow topographic feedback, the dynamics of eddies interacting with boundaries have been analyzed in the reduced-gravity setting with a vertical wall (e.g., Nof 1999, and references therein). The interaction of a lenslike anticyclone with a vertical wall involves a competition between at least three processes: the so-called image effect, which produces a poleward migration of anticyclones; a β-induced equatorward drift that becomes pronounced when the eddy encounters the western boundary; and a poleward propagation because of an ejection of mass equatorward from the eddy. In the context of a reduced-gravity lenslike eddy, these processes are essentially in balance and the eddy slowly decays as it moves into the wall without substantial meridional migration.

Recent numerical experiments by Frolov et al. (2004) included a more realistic continental shelf that is allowed to penetrate all the way into the upper layer, when isopycnals intersect bathymetry. The physical mechanism that has the most significant effect on the evolution of the anticyclonic vortex is shown to be a vortex-induced water exchange between the shallow shelf with high potential vorticity and upper-layer water at the vortex periphery with low potential vorticity over the deep ocean. The vortex interaction with secondary upper-layer cyclones that are generated by off-shelf advection of high potential vorticity results in the vortex becoming elliptic and rotating clockwise with its center following a cycloidal trajectory with a net southward drift. The characteristic pattern of vortex evolution seen in the numerical experiments can be identified in some observed cases of Loop Current eddy interactions with the western boundary in the Gulf of Mexico.

Abrupt topography penetrating all the way into the upper layer can be considered within quasigeostrophic models where the height of topography in the upper layer is small in comparison with the mean depth of the upper layer (e.g., Thompson 1993; Dewar and Leonov 2004; White and McDonald 2004). Dynamics of waves and vortices in the vicinity of finite steplike topography, with two layers of fluid on one side of the step and only one layer on the other side, were shown to be significantly different than those of more conventional models with topography occupying a small fraction of the depth of the lower layer.

Evaluation of deep-flow topographic feedback on the evolution of surface-intensified eddies is a difficult and fundamental problem; currently, there is a very limited understanding of its implications. A number of the previous studies of topographic effects on eddies have been summarized by Sutyrin (2001) and Jacob et al. (2002). An inviscid asymptotic theory was proposed by Sutyrin (2001) that allows for the description of the deep-flow pattern beneath a surface-intensified vortex on the β plane over a steep topographic slope and the subsequent estimation of its feedback on the vortex drift for an arbitrary slope orientation. However, the theory was developed for uniform and weakly nonuniform slopes, and it is not able to describe the deep flow in the presence of strongly nonuniform slope.

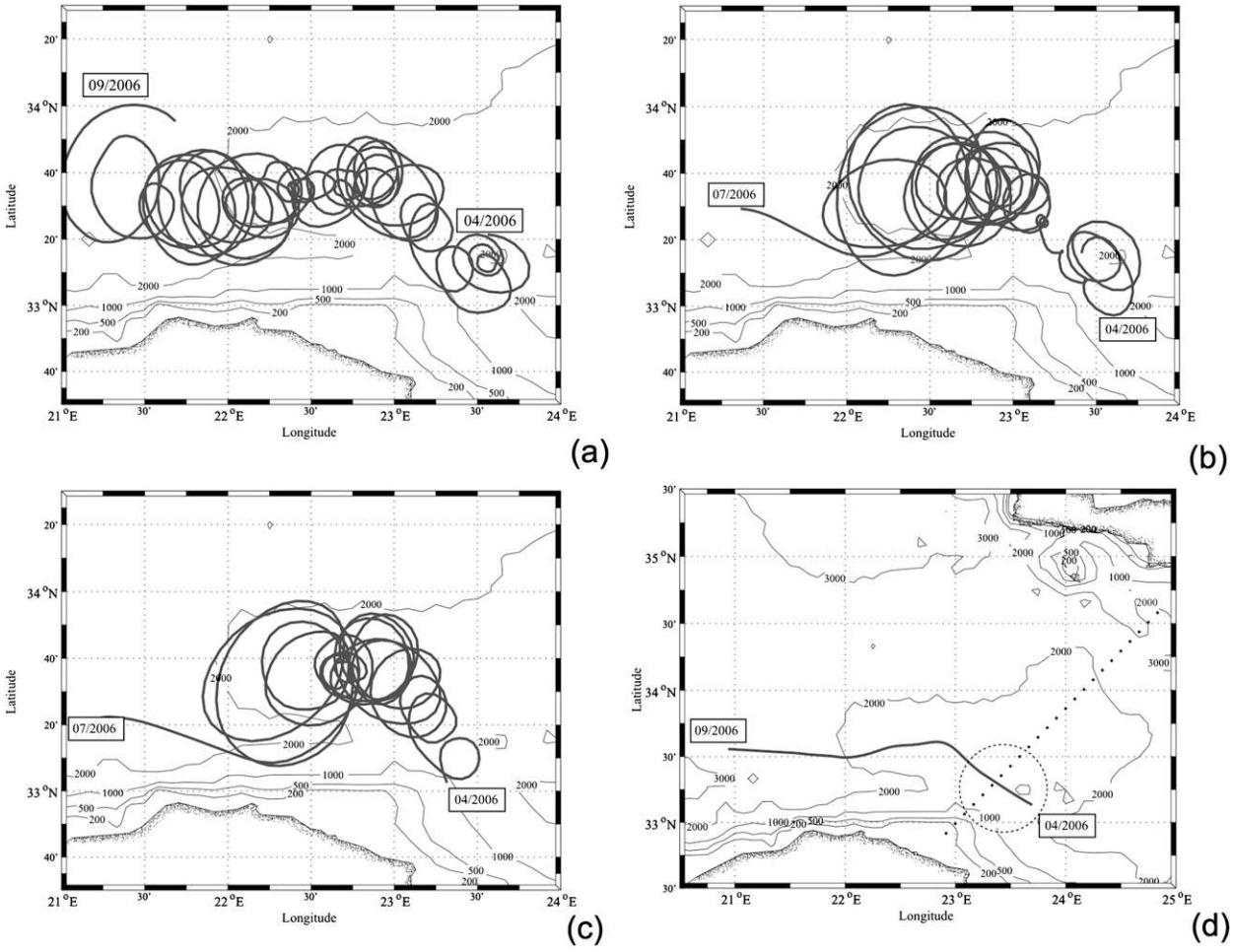

FIG. 1. Surface drifter trajectories of buoys (a) B557312, (b) B59774, and (c) B59777 trapped within the core of a large-scale LE anticyclone. (d) The mean eddy trajectory from April to September 2006 is plotted. The dots in (d) correspond to the vertical CTD profiles taken from 19 to 21 Apr.

b. This paper

The detailed sampling of an anticyclonic eddy off Libya provides strong observational basis for eddy–slope interactions. Here, we focus on the baroclinic eddy evolution near a steep continental slope and gentle continental rise using asymptotic analysis in the two-layer setup generalizing the theory by Sutyrin (2001).

The rest of the paper is organized as follows: the horizontal and vertical structures of the mesoscale anticyclone drifting along the Libyan shelf are given in section 2. The two-layer dimensionless model and the perturbation theory are formulated in section 3. In section 4, the lower-layer flow pattern and the corresponding deep-flow feedback are evaluated for a combination of steep and gentle slopes. Numerical modeling is described in section 5. The discussion and conclusions are presented in section 6.

2. Structure and trajectory of a mesoscale anticyclone along the Libyan shelf

The EGYPT-1 campaign took place in April 2006. The infrared satellite imagery was analyzed in near–real time to retrieve information on the mesoscale structures. It enabled sampling along the Libyan shelf of a mesoscale anticyclone [Libyan eddy (LE)] with a CTD transect (Fig. 1d) and surface drifters (information available online at http://poseidon.ogs.trieste.it/sire/drifter/egitto_0406_sem.html). Among them, three drifters remain trapped in the core of the LE anticyclone for several months.

Unlike the usual eddies generated by the instability of the Libyo-Egyptian Current that drift eastward (Hamad et al. 2005; Millot and Taupier-Letage 2005), both the drifters and the infrared satellite images showed that the LE anticyclone drifted westward for more than one year

(Taupier-Letage 2008). The analysis of these in situ observations is presented below.

a. Surface drifters and eddy trajectories

The trajectories of the three surface drifters (released between 10 and 11 April 2006) that remained trapped in the LE anticyclone are shown in the Fig. 1. The Argos positioning system provides their latitudes and longitudes with a high temporal frequency. The kriging method (Poulain and Zambianchi 2007) was used to filter the dataset and extract the position (X_i, Y_i) and the instantaneous speed vector V_{-i} of the drifters every six hours. One buoy, nB57312, remained trapped in the core of the LE anticyclone from April to September (Fig. 1a), whereas the other two buoys (nB59774 and nB59777) remained trapped from April to July (Figs. 1b,c). The drifters looped inside the eddy with approximately the same mean period of five days. Hence, when we filter out these rapid oscillations on both the latitude and the longitude dataset for the three drifters, we can extract the slow evolution of the eddy center. The trajectory of the LE anticyclone is then interpolated. The westward drift of the LE anticyclone, following the Libyan shelf, is shown in Fig. 1d. Surprisingly, the distance between the vortex center and the −200-m bathymetry remain almost constant $L \sim 55$–65 km. The LE anticyclone propagated westward, along a steep shelf bathymetry, with a mean speed of $V_{\mathrm{LE}} \simeq 1$–2 km day^{-1}.

b. The core rotation of the LE anticyclone

Using the eddy trajectory plotted in Fig. 1d, we could calculate for each successive position (X_i, Y_i) the radial distance R_i from the drifter to the eddy center. In Fig. 2, we plot the data pair (R_i, V_i) measured every six hours during the five-month period (April–September) when the drifter nB57312 remained trapped inside the eddy (Fig. 1a). The intermittency of the local wind stresses or the small-scale wave activity induces dispersion in the drifter dynamics and a wide range of R_i values are explored while the drifters loop inside the eddy. In the first approximation, we could assume a steady solid body rotation of the vortex core during this 5-month period and fit these data with a linear relation $V_i = \Lambda R_i$. According to Fig. 2, we get an angular rotation rate $\Lambda \simeq 10^{-5}$ rad s^{-1} and the maximum velocity seems to be reached for $R \simeq 30$–35 km. The core vorticity $\zeta_{\mathrm{LE}} = 2\Lambda \simeq 2\,10^{-5}$ rad s^{-1} $\simeq 0.25\,f_0$ remains moderate in comparison with the local Coriolis parameter $f_0 = 7.810^{-5}$ rad s^{-1}.

c. The vertical structure of the LE anticyclone

The 30 CTD profiles were taken between 19 and 21 April 2006. In Fig. 1d, we plot the locations of these CTD profiles and the estimated position of the vortex center at that time according to the drifters trajectories analysis in section 2a. A 35-km circle indicates the radius of maximum velocity or, in other words, the core of the LE anticyclone. This CTD transect crosses the eddy close to its center. The horizontal sampling of this transect is about 10 km, whereas the vertical resolution is close to 1 m. From these high-resolution measurements, we extracted a typical density cross section of the vortex (Fig. 3a). The unperturbed thermocline depth is about 150 m, whereas it could reach 300 m in the vicinity of the vortex center. Hence, the relative isopycnal deviation induced by the LE anticyclone is finite. For a geostrophically balanced vortex, such a large isopycnal deviation could only be induced by an eddy that is large enough in comparison to the deformation radius R_d of the first baroclinic mode. Indeed, if we estimate this latter quantity according to the vertical stratification outside the anticyclone, we get $R_d \simeq 13$ km, which is significantly smaller than the core vortex size $R \simeq 30$–35 km. Moreover, we add the seafloor bathymetry along the transect to Fig. 3a. The center of this surface-intensified eddy seems to be located above the breaking point of the shelf topography (Fig. 3a). The slope of the sea shelf is about $p = 10\%$, which is much steeper than the isopycnal slope (~0.5%) in the anticyclonic vortex (Fig. 3b). Hence, the LE anticyclone drifts along a steep shelf topography.

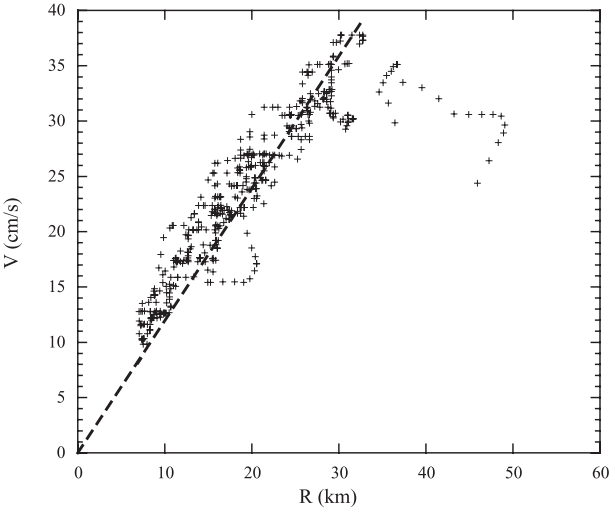

FIG. 2. Instantaneous buoy velocities as a function of the radial distance to the vortex center.

d. Dimensional analysis

According to these in situ measurements, we could accurately quantify the various dynamical parameters that control the dynamics and the eddy trajectory. Both the standard Rossby number $\mathrm{Ro} = V_0/fL \simeq 0.12$ and the

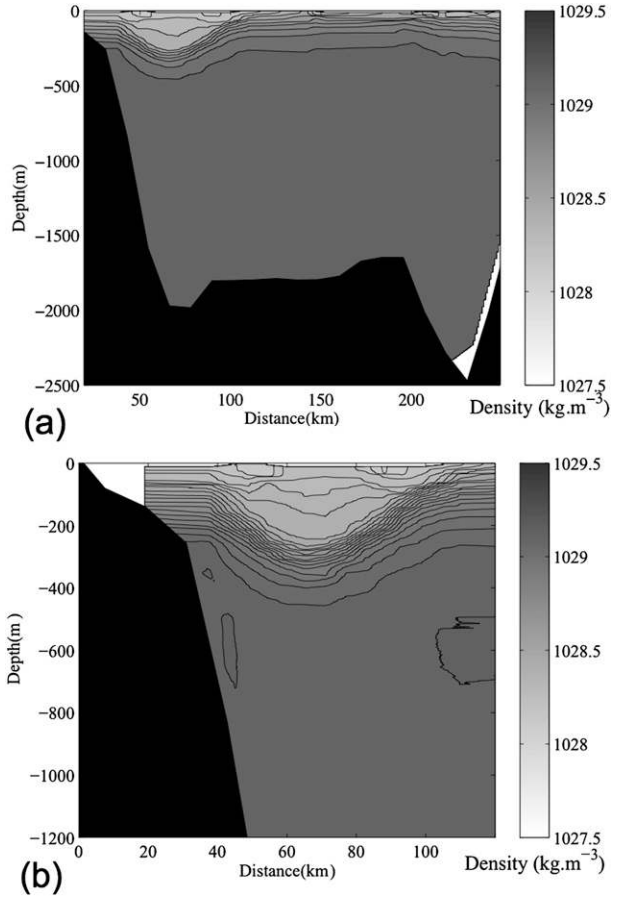

FIG. 3. (a) Vertical density cross section of the LE anticyclone along the seafloor bathmetry. (b) Isopycnal devations of the anticyclone close to the steep shelf slope.

dynamical Rossby number $\varepsilon = \zeta_{LE}/f \simeq 0.25$ are small, where V_0 is the maximum eddy velocity, R is the characteristic radius, and ζ_{LE} is the core vorticity. Hence, the LE anticyclone satisfies the geostrophic balance at the first order of approximation. Besides, the typical eddy radius R is significantly larger than the local deformation radius $R_d = 13$ km, leading to a small Burger number $\mathrm{Bu} = (R_d/R)^2 \simeq 0.16$. The Burger number of a coherent vortex is directly proportional to the kinetic to potential energy ratio and therefore, the potential energy stored in the vortex remains large in comparison with its kinetic energy. We also introduce $\delta = h_0/H_0$ the aspect ratio of the upper thermocline thickness $h_0 \simeq 150$ m to the depth H_0 of the barotropic lower layer. For a two-layer system, the layer thickness ratio δ controls the dynamical interactions between the two layers. The growth rates of baroclinic unstable modes, if there are any, are strongly reduced for small values of δ. Besides, according to Cushman-Roisin et al. (1992), the upper layer is not affected at the first order of approximation by the lower dynamics when $\delta \ll \min(1, \mathrm{Bu}^2)$. However, even if the layer thickness ratio $\delta \simeq 0.08$ is small, this value is not negligible in comparison with the square of the Burger number $\mathrm{Bu}^2 \simeq 0.02$–$0.03$. Hence, the lower-layer motion may nevertheless play a significant role in the upper-layer dynamics, as demonstrated later. The parameter C quantifies the amplitude of the vortex drift V_{LE} in comparison with the maximum eddy velocity V_0. In other words, C is related to the slow evolution of the vortex in comparison with the eddy turnover time. According to the small value of $C \simeq 0.04$, the LE anticyclone evolves slowly and is expected to have closed streamlines and a large amount of water trapped in its core. The last parameter To measures the relative amplitude of the shelf slope in comparison to the isopycnal slopes induced by the geostrophic motion of the surface-intensified vortex. All of these dynamical parameters are summarized in Table 1.

As far as the westward drift speed of a mesoscale vortex is concerned, we should estimate the maximum phase speed of Rossby waves associated to the first baroclinic mode. According to the local deformation radius $R_d \simeq 13$ km, this phase speed is about $V_\beta = \beta R_d^2 \simeq 0.2$ km day^{-1}. If we consider the westward drift of an isolated anticyclone in a reduced-gravity shallow-water model (Nezlin and Sutyrin 1994; Stegner and Zeitlin 1995, 1996), nonlinear effects induced by the finite isopycnal deviation may lead to a supercritical drift speed of $V_d \simeq V_\beta(1 + a\lambda)$, where a is a geometrical factor that depends on the eddy shape. If we take $a \simeq 1$ in the first approximation, we get $V_d \simeq 0.4$ km day^{-1}. Hence, if we do not take into account the bottom topography or the influence of the coastline, the nonlinear beta drift underestimates the measured drift velocity $V_{LE} \simeq 1.3$–2 km day^{-1} of the LE anticyclone.

3. A two-layer model

a. Two-layer equations

We consider a two-layer rotating fluid in the Boussinesq, hydrostatic, rigid-lid, and β-plane approximations along a steep shelf topography (Fig. 4). The layer densities

TABLE 1. Dimensionless parameters of the mesoscale LE anticyclone.

$\mathrm{Ro} = V_0/fR$	$\mathrm{Bu} = (R_d/R)^2$	$\lambda = \Delta h/h_0$	$\alpha = h_0/R$	$\delta = h_0/H_0$	$C = V_{LE}/V_0$	$\mathrm{To} = s/\alpha$
0.1–0.15	0.14–0.18	~1	~0.005	~0.08	0.03–0.06	~20

are ρ_j, the depths are h_j, the pressure field is p_j, and the velocity vector is $\mathbf{v}_j = (u_j, v_j)$, where $j = 1$ and $j = 2$ represent variables in the upper and the lower layers, respectively.

First, we nondimensionalize the variables as follows:

$$(\hat{X}, \hat{Y}) = (X, Y)/R, \quad \hat{t} = tV_0/R, \quad \hat{f} = f/f_0 \quad \text{and} \quad (1)$$

$$(\hat{u}_j, \hat{v}_j) = (u_j, v_j)/V_0, \quad \hat{h} = h_1/h_0, \quad \hat{h}_2 = h_2/H_0,$$
$$\hat{H}_T = H_T(y)/H_0, \quad \hat{p}_j = p_j/\rho_j g_0, \quad (2)$$

where R and $V_0 = \mathrm{Ro} f_0 R$ are the eddy radius and the characteristic eddy velocity, respectively; h_0 is the mean upper-layer depth; $g' = (\rho_2 - \rho_1)g/\rho_1$ is the reduced gravity; and f_0 is the Coriolis parameter at the reference latitude. We introduce here the standard horizontal scale $R_d = \sqrt{g'h_0}/f_0$, which corresponds to the baroclinic deformation radius when $\delta = h_0/H_0 \ll 1$ and $\rho_2 - \rho_1 \ll \rho_1$. Finite interface deviation could occur under geostrophic balance when $\mathrm{Ro} = \mathrm{Bu} = (R_d/R)^2 \ll 1$ [e.g., the LE anticyclone or cyclogeostrophic balance when $\mathrm{Ro} = \mathrm{Bu} = (R_d/R)^2 \simeq 1$]. Hence, in this section, we do not make any assumptions about the Rossby number Ro or the two-layer aspect ratio δ, and the calculation remains valid if these parameters are equal to unity.

After the hats for the nondimensional variables are dropped, the momentum and continuity equations become

$$\mathrm{Ro}[\partial_t \mathbf{v}_j + (\mathbf{v}_j \cdot \nabla)\mathbf{v}_j] + f\,\mathbf{k} \times \mathbf{v}_j = -\nabla p_j, \quad (3)$$

$$\partial_t h_j + \nabla \cdot (h_j \mathbf{v}_j) = 0, \quad \text{and} \quad h_2 = H_T(Y) + \delta(1 - h_1), \quad (4)$$

where ∇ is the horizontal gradient operator and $\mathbf{k}$ is the vertical unit vector. The pressure and upper-layer thickness gradients are related by the hydrostatic equation

$$\nabla h_1 = \nabla(p_1 - p_2). \quad (5)$$

Both the horizontal dissipation and the bottom friction are neglected in this two-layer model. Hence, the potential vorticity q_j is conserved in fluid parcels for each layer:

$$(\partial_t + \mathbf{v}_j \cdot \nabla) q_j = 0 \quad \text{and} \quad q_j \equiv \frac{f + \mathrm{Ro}\,\mathbf{k} \cdot \nabla \times \mathbf{v}_j}{h_j}. \quad (6)$$

The right-hand coordinate system corresponds to the depth topography $H_T(Y)$, with the y axis directed offshore and the x axis parallel to the isobath. Thus, the dimensionless Coriolis parameter is $f = 1 + \beta Y$ and $\beta = f'R/f_0$, where f' is the dimensional northward gradient of the Coriolis parameter. Assuming a zonal boundary at $Y = -L$, where $L = L_c/R$ is the nondimensional distance from the vortex center to the coast, we apply there the free-slip boundary conditions $u_j = 0$.

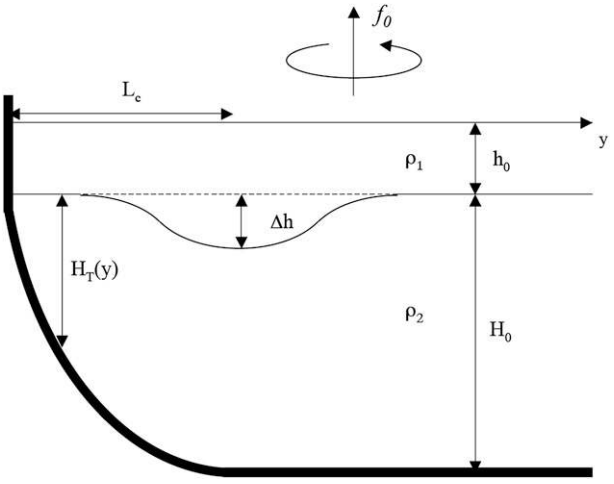

FIG. 4. Two-layer model of a surface-intensified anticyclone along a steep shelf bathymetry.

Typically, $\beta \simeq 10^{-2}$, and it is considered to have a small value here. A perturbation expansion in β was used by Sutyrin (2001) to construct a formula for the deep-flow feedback on the upper-layer vortex drift over weakly nonuniform sloping topography. Here, we use the similar methodology to consider the vortex drift along a strongly nonuniform sloping topography, also taking into account a weak image effect and assuming a zonal boundary.

b. Perturbation theory and the deep-flow structure

When $\beta = 0$ (the f plane) and $L = \infty$ (far from the wall), for any circular vortex in the upper layer,

$$p_1 = h_1 - 1 = P(r), \quad \mathbf{V}_1 = \Omega(r)(-Y, X), \quad \text{and}$$
$$\frac{dP}{dr} = r\Omega(1 + \Omega) \quad (7)$$

with no motion in the lower layer ($\mathbf{v}_2 = 0$) is a stationary solution of the two-layer system. The variables $P(r)$ and $\mathbf{V}_1(r)$, with $r = \sqrt{X^2 + Y^2}$, correspond here to the pressure and velocity fields, respectively, that are associated with this steady circular vortex. The presence of the image and β effects induces a translation of the vortex center and could also disperse the initial structure (Firing and Beardsley 1976; Masuda et al. 1990).

We assume here that a coherent and steady drifting solution could be reached in the two-layer system. The characteristic drift speeds resulting from the image and β effects are given by $2L|\Omega(2L)| \ll 1$ and $V_\beta/V_0 = \beta(\mathrm{Bu}/\mathrm{Ro}) \ll 1$, respectively. In both cases, we consider a

small drift speed in comparison with the characteristic eddy velocity, leading to a perturbation expansion in $C = V_d/V_0 \ll 1$. In this case, we assume that the circular vortex solution [$P(r)$ and $\mathbf{V}_1(r)$] will be slightly distorted by the weak β effect, the wall effect, and the lower-layer bottom topography.

Therefore, we seek a stationary solution in the coordinate system ($x = X + Ct$, $y = Y$), translating alongslope with the velocity $(-C, 0)$. To satisfy the boundary condition, the image effect is taken into account by adding the opposite sign vortex in the upper layer at the distance $y = -2L$ from the center of coordinates, which generates additional flow on the order ε. For a sufficiently large distance from the coast, the velocity $\varepsilon\tilde{\mathbf{V}}$ and the pressure deviation $e\tilde{P}$ induced by the image effect (at the vortex location) will be weak in comparison with the circular vortex flow:

$$\varepsilon\tilde{\mathbf{V}} = \Omega(\tilde{r})(y + 2L, -x), \quad \tilde{r}^2 = x^2 + (y + 2L)^2 \quad \text{and}$$
$$\varepsilon\frac{d\tilde{P}}{d\tilde{r}} = \tilde{r}\Omega(1 - \Omega). \tag{8}$$

As mentioned before, the drifting velocity of the LE anticyclone measured in the EGYPT campaign is small in comparison with the typical eddy velocity of the surface layer. Therefore, we assume $C \sim \varepsilon \ll 1$ leads to the following asymptotic expansions:

$$p_1 = P(r) - \varepsilon\tilde{P}(\tilde{r}) + C\eta + C\psi + O(C^2) \quad \text{and}$$
$$h_1 = 1 + P(r) - \varepsilon\tilde{P}(\tilde{r}) + C\eta + O(C^2), \tag{9}$$

where p_1 is the upper-layer pressure sum of the circular vortex pressure P, the pressure of the circular image vortex $\varepsilon\tilde{P}$, the interface deviation $C\eta$ induced by the steady translation, and the lower-layer pressure $C\psi$. We assume here that the steady drifting vortex structure trapped fluid parcels in the upper layer but not in the deep lower layer. In this case, the lower-layer velocity V_2 cannot be larger than the drifting velocity $V_d = CV_0$. Hence, we write for the velocity fields

$$\mathbf{v_1} = \Omega(r)(-y, x) + \varepsilon\tilde{\mathbf{V}} + \mathbf{C}\mathbf{v} + O(C^2) \quad \text{and}$$
$$\mathbf{v_2} = C\mathbf{k} \times \nabla\psi, \tag{10}$$

where υ_1 is the upper-layer velocity sum of the circular vortex velocity $\mathbf{V_1}(r)$, the image vortex velocity $\varepsilon\tilde{\mathbf{V}}$, and the velocity contribution $\mathbf{Cv}$ due to the steady translation

$$p_2 = C\psi + O(C^2, \beta) \quad \text{and}$$
$$h_2 = H_T(Y) - \delta P(r) + \delta\varepsilon\tilde{P}(\tilde{r}) - \delta C\eta + O(C^2). \tag{11}$$

The steadily translating perturbation given by (9)–(11) at leading order satisfies the following system, obtained by linearizing the original equations:

$$\mathbf{k} \times \mathbf{v} + \frac{\beta}{C}y\mathbf{k} \times \mathbf{V_1} + \nabla(\eta + \psi) = -\mathrm{Ro}\{\partial_x\mathbf{V_1} + [(\mathbf{v} + \tilde{V}) \cdot \nabla]\mathbf{V}_1 + (\mathbf{V}_1 \cdot \nabla)(\mathbf{v} + \tilde{V})\} \tag{12}$$

and

$$\nabla \cdot [(1 + P)\mathbf{v} + \eta\mathbf{V_1}] = -\partial_x P + \frac{\varepsilon}{C}\nabla \cdot [\tilde{P}(\tilde{r})\mathbf{V_1} - (1 + P)\tilde{V}]. \tag{13}$$

The upper-layer perturbations can be found in a manner similar to that proposed by Benilov (1996) in the reduced-gravity approximation with the lower layer at rest. However, the lower-layer flows could be derived from the Lagrangian conservation of the potential vorticity (6):

$$q_2 = \frac{1}{H_T(Y) - \delta P} + O(C\mathrm{Ro}, \beta) \quad \text{and} \tag{14}$$

$$D_t q_2^{-1} = J[C\psi - Cy, H_T(y) - \delta P(r)] + O(C^2\mathrm{Ro}, C\beta) = 0. \tag{15}$$

Hence, at the first order of approximation, the deep-flow structure depends only on the first-order circular vortex solution $P(r)$ and the bathymetry $H_T(y)$. This implicit relation can then be easily integrated along characteristics to find an explicit expression for the lower-layer flow pattern but, crucially, only when there are no closed contours of the lower-layer streamfunction. In such a case, we get

$$\psi = y - H_T^{-1}[H_T(y) - \delta P(r, t)] + O(C\mathrm{Ro}, \beta). \tag{16}$$

c. Integral constraints and the deep-flow feedback

As pointed out by Sutyrin (2001), it is not necessary to calculate the upper-layer perturbations in detail to find the propagation speed. Instead, it can be found from integral constraints in a manner similar to that proposed by Killworth (1983) and Nof (1983), assuming that the eddy is localized (i.e., the flow decays fast enough with r, and all the following integrals are finite). By multiplying the mass conservation Eq. (13) by x and integrating by parts over the entire area, we obtain

$$M = -\int\left\{(1 + P)(u + \frac{\varepsilon}{C}\tilde{u}) + \left[\eta - \frac{\varepsilon}{C}\tilde{P}(\tilde{r})\right]U_1\right\}dx\,dy = 2\pi\int Pr\,dr = 2\pi\int(h_1 - 1)r\,dr, \tag{17}$$

where, at the first order of approximation, M is the mass excess of the upper-layer vortex.

The momentum perturbation integral in (17) can be expressed using the momentum Eq. (12) multiplied by $1 + P$ and integrated by parts over the entire area:

$$\int [(1+P)u + \eta U_1]dx\,dy = \frac{\beta}{C}\int (1+P)\Omega y^2\,dx\,dy - \int (1+P)\partial_y\psi\,dx\,dy. \quad (18)$$

Here, we use (9) to express the first integrals in the right-hand side by the sum of the mass excess M and the potential energy E_p:

$$\int P\Omega x^2\,dx\,dy = \int P\Omega y^2\,dx\,dy = \pi\int P\frac{dP}{dr}r^2\,dr = -E_p + O(\mathrm{Ro}) \quad \text{and} \quad (19)$$

$$\int \Omega x^2\,dx\,dy = \int \Omega y^2\,dx\,dy = \pi\int \frac{dP}{dr}r^2\,dr = -M + O(\mathrm{Ro}), \quad (20)$$

where $E_p = \pi\int P^2 r\,dr$.

Finally, at the first order of approximation, we obtain

$$C = \beta\left(1 + \frac{E_p}{M}\right) + \frac{\varepsilon}{M}\int [\tilde{P}(\tilde{r})U_1 - (1+P)\tilde{u}]dx\,dy + \frac{C}{M}\int (1+P)\partial_y\psi\,dx\,dy. \quad (21)$$

The first term describes the β drift in the reduced-gravity approximation found by Killworth (1983) and Nof (1983). The ratio E_p/M is positive for anticyclones and negative for cyclones, and it provides the essential difference between the evolution of cyclonic and anticyclonic eddies (e.g., Nezlin and Sutyrin 1994). The second part describes the image effect, whereas the third term describes an additional drift resulting from the lower-layer flow feedback, which is the focus of this study.

From (21), we see that the evaluation of the topographic feedback on the vortex propagation consists of two steps. First, we have to obtain the solutions to (15) describing the components of the deep-flow pattern generated by the along-slope vortex drift depending on the interface shape. Second, inserting the solution for ψ into (21) allows us to calculate the drift velocity modified by the deep-flow feedback.

4. Deep-flow feedback

To calculate the deep-flow feedback on a surface-intensified vortex, we choose here, for simplicity, an exponential shelf topography:

$$H_T(Y) = 1 - \exp[-\delta\mathrm{To}(y + L)] \quad \text{where } y \geq -L. \quad (22)$$

This bottom slope is controlled by three parameters: the two-layer aspect ratio δ, the topographic slope parameter To, and the nondimensional distance from the vortex center to the coast L. According to the relation (16), we get the streamfunction in the coastal frame

$$\psi = \frac{1}{\delta\mathrm{To}}\log\{1 + \delta P(r)\exp[\delta\mathrm{To}(y+L)]\}. \quad (23)$$

This low-layer flow corresponds to an anticyclonic circulation with along-slope velocity

$$\frac{\partial\psi}{\partial y} = \frac{1}{\mathrm{To}}\frac{\partial_y P + \delta\mathrm{To}P}{\exp[-\delta\mathrm{To}(y+L)] + \delta P}. \quad (24)$$

The center of the deep-flow circulation is shifted offshore by the distance defined by $\partial_y P = -\delta\mathrm{To}P$. We define the acceleration coefficient γ corresponding to the additional drifting velocity from the deep-flow feedback according to (21):

$$C = (1+\gamma)\left\{\beta\left(1 + \frac{E_p}{M}\right) + \frac{\varepsilon}{M}\int [\tilde{P}(\tilde{r})U_1 - (1+P)\tilde{u}]dx\,dy\right\}, \quad (25)$$

where a positive (negative) value of γ corresponds to an increase (decrease) of the steady drifting velocity induced by the deep-layer bottom topography.

For an exponential shelf topography, the acceleration coefficient γ satisfies (24):

$$\frac{\gamma}{1+\gamma} = \frac{1}{M}\int (1+P)\frac{\partial_y P + \delta\mathrm{To}P}{\mathrm{To}\{\exp[-\delta\mathrm{To}(y+L)] + \delta P\}}\,dx\,dy. \quad (26)$$

This integral formula allows us to estimate the acceleration coefficient, depending on the circular vortex structure $P(r)$ and the parameters To and δ. In what follows, we take a Gaussian upper-layer vortex $P = \lambda\exp(-\frac{1}{2}r^2)$. For small aspect-ratio parameter $\delta \ll 1$, we get, at the first order of approximation and in the lower layer, a Gaussian pressure field shifted offshore by the distance δTo:

$$\psi = \frac{\lambda}{\mathrm{To}}\exp\left[\delta\mathrm{To}\left(L + \frac{1}{2}\delta\mathrm{To}\right)\right]\exp\left\{-\frac{1}{2}[x^2 + (y - \delta\mathrm{To})^2]\right\} \quad (27)$$

Typical streamlines plotted in the steady drifting frame are shown in Fig. 5 for both the upper and lower

layers. According to the closed streamlines of Fig. 5a, the surface-intensified vortex trapped fluid within its core, whereas the lower-layer fluid parcels simply deviated offshore (Fig. 5b) without trapping any fluid. The acceleration coefficient γ is then given by the relation

$$\frac{\gamma}{1+\gamma} = \frac{\lambda}{M}\int_{-L}^{+\infty}(\delta\mathrm{To} - y)dy \int_{-\infty}^{+\infty} dx \frac{\left[\exp\left(-\frac{r^2}{2}\right) + \lambda\exp(-r^2)\right]}{\mathrm{To}\left\{\exp[-\delta\mathrm{To}(y+L)] + \delta\lambda\exp\left(-\frac{r^2}{2}\right)\right\}}, \tag{28}$$

where $M = \lambda\sqrt{2\pi}\int_{-L}^{+\infty}\exp(-y^2/2)dy$.

We then study the variations of the acceleration coefficient γ according to the dimensionless parameters λ, δ, and To. According to Fig. 6a, we have shown that for small values of the two-layer aspect ratio ($\delta \ll 1$), the drifting speed acceleration is mainly controlled by the product δTo. Hence, when $\delta\mathrm{To} \simeq 2$, the deep-flow feedback induced by the steep shelf topography could increase the vortex drift by 100% or even more. When δTo becomes finite, the potential voricity gradient in the lower layer, because of the shelf slope, is of the same order of magnitude as the potential vorticity gradient induced by the upper-layer vortex. In such a case, the lower-layer retroaction becomes significant and the acceleration coefficient increases strongly for steeper shelf slopes. The relative amplitude of the isopycnal displacement λ, which is related to the relative size of the vortex in comparison with the local deformation radius, also controls the acceleration coefficient (Fig. 6b).

5. Numerical simulations

The previous integral relations (21) and (26) assume that a steady drifting vortex could be reached by the two-layer system. However, the existence and/or stability of a coherent steady state cannot be guaranteed by the center-of-mass relation. Topographic Rossby or Kelvin wave radiations and/or instabilities could strongly affect an initial vortex along the steep topography. To investigate the time evolution and the robustness of an initially isolated vortex analogous to the LE anticyclone (observed during the EGYPT campaign), we perform some numerical simulations with a geostrophic vorticity intermediate two-layer model (Sutyrin et al. 2003). This intermediate model does not reproduce the dynamic of inertia–gravity waves and some ageostrophic instabilities. However, for a large-scale geostrophic vortex (i.e., small Rossby number), these fast components of motion should have a weak influence on the slow evolution of the eddy.

a. Scaling and derivation of intermediate equations

We consider a vortex with maximum velocity $V_m \approx 0.4$ m s^{-1} at the radius $R_m \approx 40$ km. Choosing $f_0 \approx 8 \times 10^{-5}$ s^{-1}, we find that the Rossby number, which characterizes eddy strength relative to the planetary vorticity, is

$$\mathrm{Ro} \equiv \frac{V_m}{f_0 R_m} \approx 0.15. \tag{29}$$

Given a typical reduced gravity $g' \approx 0.01$ m s^{-1}, a typical upper-layer depth $h_0 \approx 150$ m, and assuming the eddies are in geostrophic balance at leading order, we find that the ratio of the interface displacement to the upper-layer depth,

$$\frac{f_0 V_m R_m}{g' h_0} \approx 1. \tag{30}$$

These nondimensional parameters indicate that the flow is essentially in geostrophic balance but that depth variations in the upper layer cannot be assumed small. This combination suggests an ''intermediate'' (between quasigeostrophic and primitive) simplification of the momentum Eq. (3). Here, we use an expansion in the Rossby number in the form first suggested by Sutyrin and Yushina (1986) and generalized for the multilayer settings by Sutyrin et al. (2003). Under this approximation, the leading order flow is geostrophic,

$$\boldsymbol{v}_g = \mathbf{k} \times \nabla p, \tag{31}$$

and the next order flow is expressed as

$$\mathbf{v} = \frac{1}{f + \zeta_g}(\mathbf{k} \times \nabla B - \nabla \partial_t p), \tag{32}$$

where $\zeta_g = \nabla^2 p$ is the geostrophic vorticity and $B = p + \boldsymbol{v}_g^2/2$ is the geostrophic Bernoulli function. Inserting the expression (32) into the continuity Eq. (4) yields a

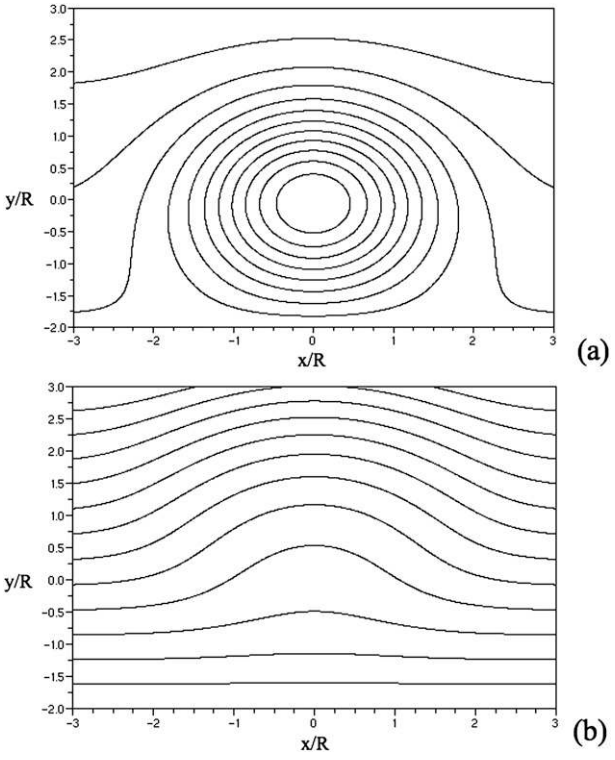

FIG. 5. (a) Upper- and (b) lower-layer streamlines in the steady drifting frame for a Gaussian vortex having similar parameters to the LE anticyclone: $c = 0.7$, $\delta = 0.08$, To = 20, and $L = 2$.

predictive system of equations for p that involves only the geopotential field

$$(-1)^j \partial_t h_1 + \nabla \cdot (PT_j \nabla \partial_t p_j) = J(B_j, PT_j) + (j-1) b \nabla^2 p_2, \tag{33}$$

where $PT = h/(f + \zeta_g)$ is the potential thickness (inverse potential vorticity), which is also conserved in fluid parcels moving with velocity described by (32). This geostrophic vorticity intermediate model was shown to be the most accurate among the various forms of the general geostrophic models that have been compared by Allen et al. (1990).

The vortex is initialized with a potential vorticity perturbation in the upper layer, taking into account the image effect to satisfy the boundary condition:

$$PT = \frac{P_\infty + Z(r) - Z(\tilde{r})}{f}, \tag{34}$$

$$Z(r) = A[1 - \tanh(-r^2)], \tag{35}$$

$$r = \frac{\sqrt{X^2 + Y^2}}{R_c}, \quad \text{and} \quad \tilde{r} = \frac{\sqrt{x^2 + (Y + 2L)^2}}{R_c}, \tag{36}$$

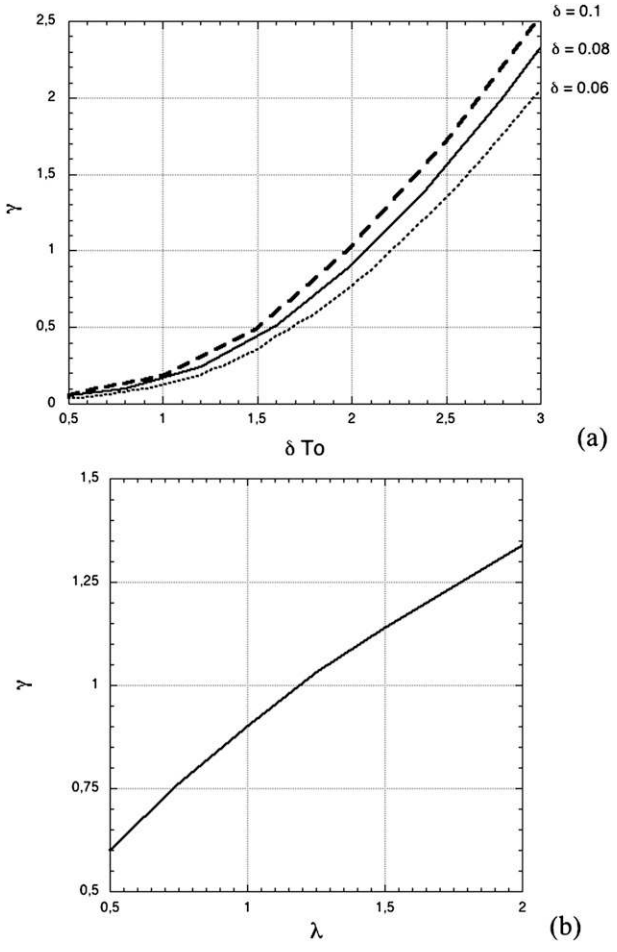

FIG. 6. Evolution of the acceleration coefficient γ (a) as a function of the product δTo (for the following values of δ: 0.06, 0.08, and 0.1) and (b) as a function of the relative isopycnal deviation parameter λ.

where the vortex core parameters $A = 2$ and $R_c = 3$ are chosen to initialize the upper-layer vortex with negative vorticity at the center and maximum velocity $v_m \approx 0.3$ at the radius $r \approx 3$ (Fig. 7). The initial velocity in the lower layer is zero.

The numerical scheme for the geostrophic vorticity intermediate equation model uses a conservative Arakawa spatial approximation for the Jacobian on the right-hand side of Eq. (33) and a second-order Adams–Bashforth approximation for each time step. The model domain is 40×27 with $\Delta x = \Delta y = 0.27$ grid resolution. Boundary conditions are no flux on the western, southern, and northern boundaries, and the eastern boundary is open to allow topographic Rossby waves to propagate out of the domain. During calculations, the domain is shifted along-slope to keep the vortex in the center of the domain. Correspondingly, unperturbed conditions are prescribed at the western boundary.

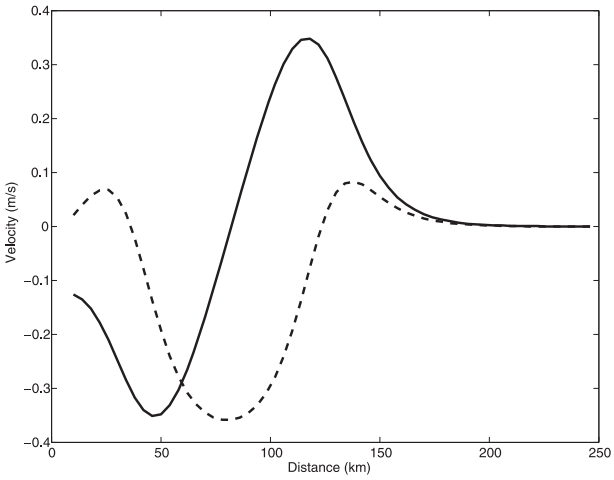

FIG. 7. Initial alongshore velocity and vorticity (dashed line) across the vortex.

b. Results of simulations

The slope in the lower layer was prescribed as $H' = S_0 + S_1\exp[-\alpha(Y + L)]$, where S_0 compensates the β effect so that $PT_2 \to$ const for large Y, whereas $S_1 = 2$ and $\alpha = 0.1$. This topographic profile is shown in Fig. 8, along with the interface, the lower-layer alongshore velocity, and the geopotential anomaly formed after the flow is reached a nearly steady state. The velocity in the lower layer is mostly negative beneath the upper-layer eddy, resulting in amplification of its westward drift. The offshore shift of the lower-layer circulation is clearly seen in Fig. 9, in which the vortex center positions are compared with the reduced-gravity simulations. The deep anticyclone corresponds qualitatively to

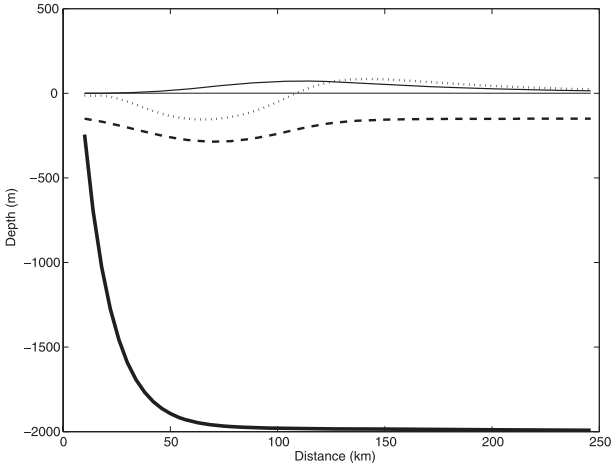

FIG. 8. The cross-isobath profiles of the ocean depth (thick line), upper-layer interface (dashed line), lower-layer geopotential (thin line), and corresponding alongshore velocity (dotted line) after six months of integration.

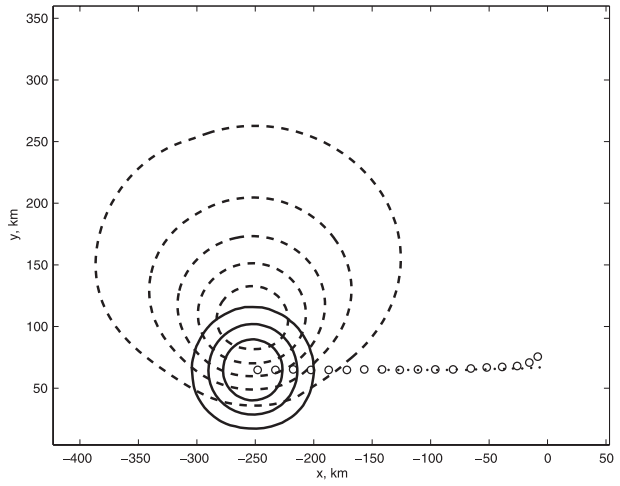

FIG. 9. The vortex center positions every 10 days for six months (circles) to compare to the reduced-gravity simulations (dots) for the same distance from the wall $L = 4.3$. Contours of interface and lower-layer pressure (dashed lines) are plotted at the final time when the solution is nearly stationary.

the analytic solution (23) and its feedback to the upper-layer vortex increases the drift speed by 85%. In dimensional units, the speed of the beta drift is about 0.5 km day $^{-1}$, whereas the image effect adds 0.3 km day^{-1} in the reduced-gravity case and the deep flow accelerates the vortex drift up to 1.5 km day^{-1}.

Note that it is steep topography that simplifies the calculation of the vortex drift in comparison with a two-layer system on the beta plane with a flat bottom considered by Benilov (2000). When starting from a circular vortex in the upper layer, the initial development of a dipolar pattern because of stretching in the lower layer is quite similar. However, an eddy over a flat bottom has westward components of translation resonating with Rossby waves, whereas over a steep slope our eddy moves in an equivalent eastward direction and reaches a steadily propagating stage described by our simple analytical solution.

6. Discussion and conclusions

Motivated by the recent in situ measurements of the EGYPT/EGITTO program, we have considered the effects of bathymetry on the propagation of intense surface-intensified vortices on a β plane in a two-layer model over nonuniformly sloping topography near the boundary. A perturbation theory is proposed for a circular vortex in the upper layer and the lower layer at rest as a basic state. The vortex propagation speed is found from the integral relations that describe the β drift and image effect in the reduced-gravity approximation, and an additional feedback is due to the lower-layer flow generated by vortex-stretching effects.

Without friction, a complete solution can be found only when all contours of the lower-layer thickness are open. Most parts of the lower-layer flow pattern can then be explained in terms of potential vorticity conservation. The stretching in the lower layer associated with β-induced and/or image-effect along-slope vortex interface migration should be balanced by a water advection generating by the deep-flow pattern. The deep flow interacts with the upper layer according to the hydrostatic relation (5) and provides an additional along-slope vortex drift, which depends on the relative isopycnal displacement of the surface vortex λ, the vertical two-layer aspect ratio δ, and the topographic slope parameter To. The asymptotic analysis shows that for steep shelves, when $\delta \ll 1$, $\mathrm{To} \gg 1$, and $\delta\mathrm{To} \sim 1$, the deep-flow feedback could double the along-slope drift velocity of the surface vortex. The stability of the steady drifting solution and the amplification of the along-slope drift velocity were confirmed by numerical simulations with the same dynamical parameters as the LE anticyclone.

The instability of the Atlantic water flow—namely, the Libyo-Egyptian Current—generates anticyclones that are observed usually drifting eastward (Hamad et al. 2005; Millot and Taupier-Letage 2005). However, we assume here that the LE anticyclone is isolated (no interaction with the background surface flow). In such a case, the steep slope effect could explain its anomalously fast westward propagation along the Libyan shelf. We show here that a weak deep-flow feedback could significantly influence the drifting velocity of a stable surface vortex along a steep shelf.

Acknowledgments. GS was funded by the NSF Division of Ocean Sciences and greatly appreciates the support and hospitality of the Laboratory of Dynamical Meteorology during his visiting professorship funded by the Ecole Normale Supérieure and the Ecole Polytechnique. The authors thank P. M. Poulain and R. Gerin (OGS, Trieste, Italy) for making the drifters data of the joint EGITTO program available. The EGYPT program received funding from INSU, LEFE/IDAO, GMMC/Mercator, and the Regional Council Provence Alpes Ctes d'Azur. Thanks are extended to the ships' crews.

REFERENCES

Allen, J. C., J. A. Barth, and P. A. Newberger, 1990: On intermediate models for barotropic continental shelf and slope flow fields. Part I: Formulation and comparison of exact results. *J. Phys. Oceanogr.,* **20,** 1017–1042.

Benilov, E. S., 1996: Beta-induced transition of strong isolated eddies. *J. Phys. Oceanogr.,* **26,** 2223–2229.

——, 2000: The dynamics of a near-surface vortex in a two-layer ocean on the beta-plane. *J. Fluid Mech.,* **420,** 277–299.

Brown, O. B., P. C. Cornillon, S. R. Emmerson, and H. M. Carle, 1986: Gulf Stream warm rings: A statistical study of their behavior. *Deep-Sea Res.,* **33,** 1459–1473.

Carnevale, G. F., R. C. Kloosterziel, and G. J. F. Van Heijst, 1991: Propagation of barotropic vortices over topography in a rotating tank. *J. Fluid Mech.,* **233,** 119–139.

Cushman-Roisin, B., G. G. Sutyrin, and B. Tang, 1992: Two-layer geostrophic dynamics. Part I: Governing equations. *J. Phys. Oceanogr.,* **22,** 117–127.

Dewar, W. K., and D. A. Leonov, 2004: Variability on steep, confined topography. *Deep-Sea Res. II,* **51,** 2973–2993.

Evans, R. H., K. S. Baker, O. B. Brown, and R. C. Smith, 1985: Chronology of warm-core ring 82B. *J. Geophys. Res.,* **90,** 8803–8811.

Firing, E., and R. C. Beardsley, 1976: The behavior of a barotropic eddy on a beta-plane. *J. Phys. Oceanogr.,* **6,** 57–65.

Fratantoni, D. M., W. E. Johns, and T. L. Townsend, 1995: Rings of the North Brazil Currents: Their structure and behavior inferred from observations and a numerical simulation. *J. Geophys. Res.,* **100,** 10 663–10 654.

Freeland, H. J., and Coauthors, 1986: The Australian Coastal Experiment: A search for coastal-trapped waves. *J. Phys. Oceanogr.,* **16,** 1230–1249.

Frolov, S. A., G. G. Sutyrin, G. D. Rowe, and L. M. Rothstein, 2004: Loop Current eddy interaction with the western boundary in the Gulf of Mexico. *J. Phys. Oceanogr.,* **34,** 2223–2237.

Grimshaw, R., D. Broutman, X. He, and P. Sun, 1994: Analytical and numerical study of a barotropic eddy on a topographic slope. *J. Phys. Oceanogr.,* **24,** 1587–1607.

Hamad, N., C. Millot, and I. Taupier-Letage, 2005: A new hypothesis about the surface circulation in the eastern basin of the Mediterranean Sea. *Prog. Oceanogr.,* **66,** 287–298.

Hamon, B., 1965: The East Australian Current 1960–1964. *Deep-Sea Res.,* **12,** 899–921.

Jacob, J. P., E. P. Chassignet, and W. K. Dewar, 2002: Influence of topography on the propagation of isolated eddies. *J. Phys. Oceanogr.,* **32,** 2848–2869.

Kamenkovich, V. M., Y. P. Leonov, D. A. Nechaev, D. A. Byrne, and A. L. Gordon, 1996: On the influence of bottom topography on the Agulhas eddy. *J. Phys. Oceanogr.,* **26,** 622–643.

Killworth, P. D., 1983: On the motion of isolated lenses on a β-plane. *J. Phys. Oceanogr.,* **13,** 368–376.

Kirwan, A. D., Jr., J. K. Lewis, A. W. Indest, P. Reinersman, and I. Quintero, 1988: Observed and simulated kinematic properties of Loop Current rings. *J. Geophys. Res.,* **93,** 1189–1198.

Kizner, Z., G. Reznik, D. Berson, and G. G. Sutyrin, 2003: The theory of the beta-plane baroclinic topographic modons. *Geophys. Astrophys. Fluid Dyn.,* **97,** 175–211.

Louis, J. P., and P. S. Smith, 1982: The development of the barotropic radiation field of an eddy on a slope. *J. Phys. Oceanogr.,* **12,** 56–73.

Masuda, A., K. Marubayashi, and M. Ishibashi, 1990: A laboratory experiment and numerical simulation of an isolated barotropic eddy with topographic β. *J. Fluid Mech.,* **213,** 641–659.

McDonald, N. R., 1998: The motion of an intense vortex near topography. *J. Fluid Mech.,* **367,** 359–377.

Millot, C., and I. Taupier-Letage, 2005: Circulation in the Mediterranean Sea. *The Mediterranean Sea,* A. Saliot, Ed., Vol. 5, *The Handbook of Environmental Chemistry,* Springer-Verlag, 29–66.

Nezlin, M. V., and G. G. Sutyrin, 1994: Problems of simulation of large, long-lived vortices in the atmospheres of the giant planets (Jupiter, Saturn, Neptune). *Surv. Geophys.,* **15,** 63–99.

Nof, D., 1983: On the migration of isolated eddies with application to Gulf Stream Rings. *J. Mar. Res.,* **1,** 399–425.

——, 1999: Strange encounters of eddies with walls. *J. Mar. Res.,* **57,** 736–761.

Poulain, P. M., and E. Zambianchi, 2007: Surface circulation in the central Mediterranean Sea as deduced from Lagrangian drifters in the 1990s. *Cont. Shelf Res.,* **27,** 981–1001.

Puillat, I., I. Taupier-Letage, and C. Millot, 2002: Algerian eddies lifetimes can be near 3 years. *J. Mar. Syst.,* **31,** 245–259.

Reznik, G. M., and G. G. Sutyrin, 2001: Baroclinic topographic modons. *J. Fluid Mech.,* **437,** 121–142.

Richardson, G., 2000: Vortex motion in shallow-water with varying bottom topography and zero Froude-number. *J. Fluid Mech.,* **411,** 351–374.

Smith, D. C., IV, 1986: A numerical study of Loop Current eddy interaction with topography in the western Gulf of Mexico. *J. Phys. Oceanogr.,* **16,** 1260–1272.

——, and J. J. O'Brien, 1983: The interaction of a two-layer isolated mesoscale eddy with bottom topography. *J. Phys. Oceanogr.,* **13,** 1681–1697.

Stegner, A., and V. Zeitlin, 1995: What can asymptotic expansions tell us about large-scale quasi-geostrophic anticyclonic vortices? *Nonlinear Processes Geophys.,* **2,** 186–193.

——, and ——, 1996: Asymptotic expansions and monopolar solitary Rossby vortices in barotropic and two-layer models. *Geophys. Astrophys. Fluid Dyn.,* **83,** 159–195.

Sutyrin, G. G., 2001: Effects of topography on the β-drift of a baroclinic vortex. *J. Mar. Res.,* **59,** 977–989.

——, and I. G. Yushina, 1986: Evolution of solitary vortices in a rotating fluid. *Fluid Dyn.,* **21,** 550–556.

——, and R. Grimshaw, 2005: Frictional effects on the deep-flow feedback on the β-drift of a baroclinic vortex over sloping topography. *Deep Sea Res. I,* **52,** 2156–2167.

——, G. D. Rowe, L. M. Rothstein, and I. Ginis, 2003: Baroclinic eddy interactions with continental slopes and shelves. *J. Phys. Oceanogr.,* **33,** 283–291.

Taupier-Letage, I., 2008: On the use of thermal infrared images for circulation studies: Applications to the eastern Mediterranean Basin. *Remote Sensing of the European Seas,* V. Barale and M. Gade, Eds., Springer Verlag, 153–164.

Thierry, V., and Y. Morel, 1999: Influence of a strong bottom slope on the evolution of a surface-intensified vortex. *J. Phys. Oceanogr.,* **29,** 911–924.

Thompson, L., 1993: Two-layer quasigeostrophic flow over finite isolated topography. *J. Phys. Oceanogr.,* **23,** 1297–1314.

Umatani, S., and T. Yamagata, 1987: Evolution of an isolated eddy near a coast and its relevance to the "Kyucho." *J. Oceanogr. Soc. Japan,* **43,** 197–203.

van Geffen, J. H. G. M., and P. A. Davies, 1999: Interaction of a monopolar vortex with a topographic ridge. *Geophys. Astrophys. Fluid Dyn.,* **90,** 1–41.

van Heijst, G. J. F., 1994: Topography effects on vortices in a rotating fluid. *Meccanica,* **29,** 431–451.

Vukovich, F. M., and E. Waddell, 1991: Interaction of a warm ring with the western slope in the Gulf of Mexico. *J. Phys. Oceanogr.,* **21,** 1062–1074.

Wang, X., 1992: Interaction of an eddy with a continental slope. Ph.D. thesis, MIT/WHOI Joint Program in Oceanography, 216 pp.

White, A. J., and N. R. McDonald, 2004: The motion of a point vortex near large-amplitude topography in a two-layer fluid. *J. Phys. Oceanogr.,* **34,** 2808–2824.